The Fingerprint of Anthropogenic Warming on Global Agriculture

Corresponding Author:
Frances C. Moore
Department of Environmental Science and Policy
2140 Wickson Hall
One Shields Ave
Davis, CA 95616 USA

fmoore@ucdavis.edu
617-233-3380

Abstract

A large literature on "detection and attribution" has now demonstrated the influence of anthropogenic greenhouse gas emissions on a range of physical climate variables (1–7). Social and economic outcomes are known to be sensitive to climate change (8, 9), but directly connecting observed changes to anthropogenic forcing is challenging (10). Here I demonstrate that changes in global productivity of maize, wheat, and rice production since 1960 can be formally attributed, with high confidence, to anthropogenic warming. Specifically, I show that there is less than 10% probability that the pattern of changes in yield growth across crops and countries would have arisen in the absence of anthropogenic warming. Although the total effect of warming is small relative to the change in yield since 1960, it has produced a distinctive fingerprint on the pattern of yield growth, characterized by a slowing of wheat yield gains in warmer areas and an acceleration of rice yields in cooler regions. The net effect has been negative, reducing global calorie production from these crops by 5.7% per year. This therefore provides early evidence that anthropogenic warming is already having a discernable effect on socio-economic systems at the global scale.

Main Text

Changes in many physical climate variables, including atmospheric temperature (1, 11), ocean heat content (6), streamflow (6), and the distribution and intensity of rainfall events (3–5), have now been detected and formally attributed to greenhouse gas emissions. Attribution of observed changes requires identifying a spatio-temporal pattern (or 'fingerprint') associated with anthropogenic climate change, demonstrating this pattern in observations, and showing that this pattern could not have arisen in the absence of anthropogenic emissions.

Many social and economic outcomes, ranging from aggregate economic productivity (12) to conflict (13) to human health (14), are thought to be sensitive to climate change. But attribution of observed changes to greenhouse gas emissions is extremely challenging: climate and weather explain only a small fraction of spatial and temporal variance in most outcomes; the response to climate drivers may be heterogeneous, non-linear, and poorly understood; observations at large geographic scales over sufficiently long time spans may be unavailable or unreliable; and the influence of many other drivers, some of which may be unobserved, confounds the climate change signal (10, 15). Only a tiny fraction of studies assessed by the IPCC dealt with observed impacts in human and managed systems, and confidence in the attribution of impacts to anthropogenic climate change ranged from very low to medium(15).

Agriculture is an economic sector that is both highly exposed and sensitive to climate change. A large literature has now established that yields respond to temperature fluctuations and that future warming will likely negatively affect agricultural productivity (16–20). Nevertheless, the dominant feature of yields in the second half of the 20th century has been a large and steady increase associated with higher use of inputs and large technological improvements (Supplementary Figure 1a). A stagnation of yield growth since the 1990s, particularly for wheat, has been widely documented (21–23), with a variety of possible explanations advanced including slowing of R&D spending due to low prices, restrictions on fertilizer use in Europe, or biophysical limits to yield (24).

Supplementary Figure 1b shows the distribution of changes in yield growth by crop and climate region between 1961-1980 and 1998-2017. The slowing of yield growth, particularly for wheat, has been concentrated in the warmest part of its growing area, while both rice and maize have seen smaller gains in the very coldest parts of their range. Growing season warming trends over growing areas have been documented in many locations (25). This observation, combined with the fact that the biological response of crops to warming is generally more positive in cold places and more negative in warm

places (26, 27), means the patterns shown in Supplementary Figure 1b are at least consistent with an emerging signal of anthropogenic warming on global yield growth.

However, causally connecting anthropogenic warming with the global pattern of changes in crop yield growth requires several steps. The observation that there has been warming over many growing areas during the growing season is not evidence that agriculture has been exposed to anthropogenic warming without a formal assessment of the likelihood of this warming occurring in the absence of greenhouse gas emissions. Natural variability at the subnational scale, even on multi-decadal time spans, is fairly large (28, 29) meaning counterfactual simulations of natural variability without greenhouse gas emissions are required to formally attribute observed warming to anthropogenic emissions. Although emergence of the anthropogenic signal in surface temperatures is well-established (11, 30), attribution of growing season temperature trends to human activity has only previously been done for western and northern Europe (31).

Second, the attribution of observed yield trends to warming requires ruling out other potential drivers. This is particularly difficult in most human and managed systems because climate fluctuations typically explain only a very small fraction of variation in outcomes. Although some previous work has estimated the effect of observed weather trends on crop yields using both empirical and process-based crop models (25, 32–38), this literature has not connected estimated impacts to observed yield trends nor attempted to distinguish the role of warming from other drivers of yield, with the limited exception of French wheat yields (39). Detection and attribution requires establishing the likelihood of observations in the absence of greenhouse gas emissions and this has not been previously done for any human or managed system at the global scale.

This paper drives an empirical crop model with temperature changes from two large ensembles of the CESM over the 20th century (LENS); one using all human and natural forcing (40 members, referred to as the "historical ensemble" in this paper) and one using all human and natural forcing except greenhouse gas emissions, which are fixed at 1920 levels (20 members, referred to as the "counterfactual ensemble" in this paper) (40). The natural variability in historical temperatures represented in the climate model ensembles is convolved with uncertainty in the yield response to temperature change and uncertainty in non-temperature drivers of yield, captured in the empirical crop model, to give distributions of possible yield trajectories between 1961 and 2017 for 287 crop-country combinations. Aggregating into a one-dimensional index designed to maximize power to detect the climate change signal, I show that the observed global, multi-crop pattern of yield trends is both consistent with historical forcing and

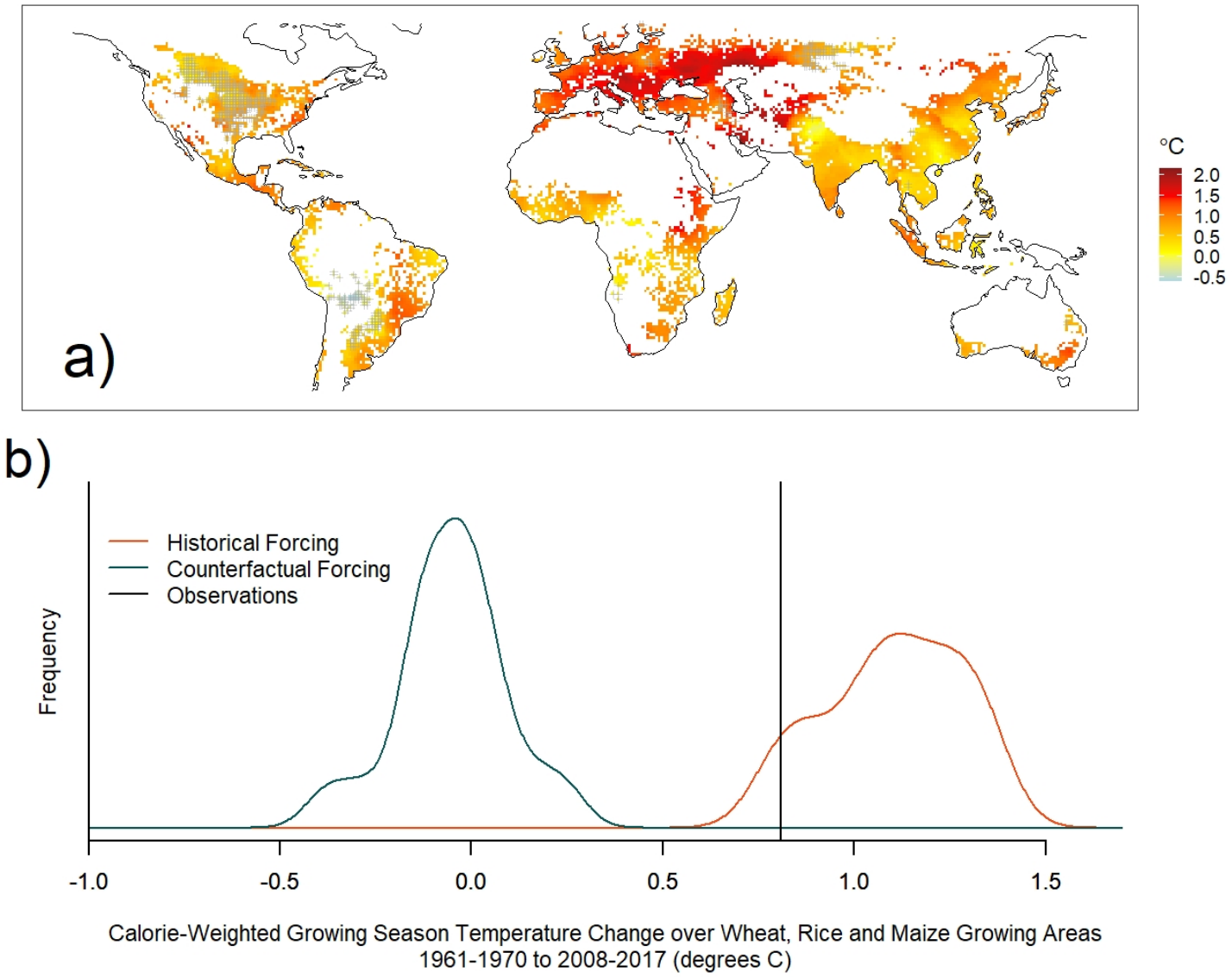

Figure One: Detection of anthropogenic warming signal over global crop areas and seasons. a) Observed change in growing season temperature over wheat, rice and maize growing areas (grid cells with >50 Ha combined in 2000 (41)) between 1961-1970 and 2008-2017 (42). Growing-season trends for the three crops are a calorie-weighted average of production for each grid cell. Grey crosses indicate areas where the observed warming is less than the 95th percentile of warming over the same period observed in the counterfactual climate model ensemble, which omits forcing from greenhouse gas emissions since 1920. b) Weighted average of growing season temperature trends for wheat, rice, and maize, aggregated based on calorie production in 2000, from the LENS ensemble under historical (40 members) and counterfactual forcing (20 members). Also shown is the observed warming of 0.8°C

inconsistent with a counterfactual world without anthropogenic warming, demonstrating that the anthropogenic signal emerged by the early 2000s and that it is now very likely (probability >90%) that anthropogenic warming has affected global crop yield development (additional details Methods, Supplementary Figure 2).

Figure 1 demonstrates that an anthropogenic warming signal has emerged over crop growing areas during the growing season. Figure 1a shows observed growing-season warming over wheat, rice, and maize growing areas between 1961-1970 and 2008-2017, the period for which global yield data exist, and a comparison to the distribution of warming trends from the counterfactual climate model ensemble. Observed growing-season warming almost everywhere can not be explained without greenhouse gas emissions, a notable exception being the "warming hole" over the US Midwest previously documented (43, 44). Aggregating to the global level on a calorie-production-weighted basis, the observed warming of 0.8°C is consistent with the distribution under historical forcing but not under the counterfactual forcing. The probability that greenhouse gas emissions were necessary and sufficient to cause the growing-season warming trend over growing areas observed during this time period (PNS, a measure of the separation of the historical and counterfactual distributions (45, 46)), is greater than 0.9999.

Supplementary Figure 3 shows the observed growing season rainfall changes over the 1961-1970 to 2008-2017 period, also compared to the counterfactual forcing distribution. Unlike temperature, an anthropogenic signal in growing-season rainfall has not emerged over many areas over this time period. This is not surprising given the substantial internal variability in decadal rainfall patterns (29, 47). The detection exercise therefore focuses only on the warming effect of anthropogenic greenhouse gas emissions, controlling for the effect of observed changes in rainfall on crop yields, but not attempting to attribute those changes to anthropogenic influence (Supplementary Figure 2).

Figure 2 show the sensitivity of crops to warming estimated in the empirical crop model. The model specification follows Lobell et al. (25) and includes country-crop fixed-effects (dummy variables), crop-year fixed-effects, and country-crop quadratic time trends that control for all time-invariant differences and smoothly varying effects on yield, as well as controls for seasonal rainfall. The model recovers now well-established features of the yield response to temperature for staple crops from both empirical and process-based models: warming is generally worse at higher than at lower temperatures, wheat and maize are more sensitive to warmer temperatures than rice, which benefits in the cooler parts of its range (26, 27, 48). Findings are also quantitatively similar to previous findings. For instance, Zhao et al.

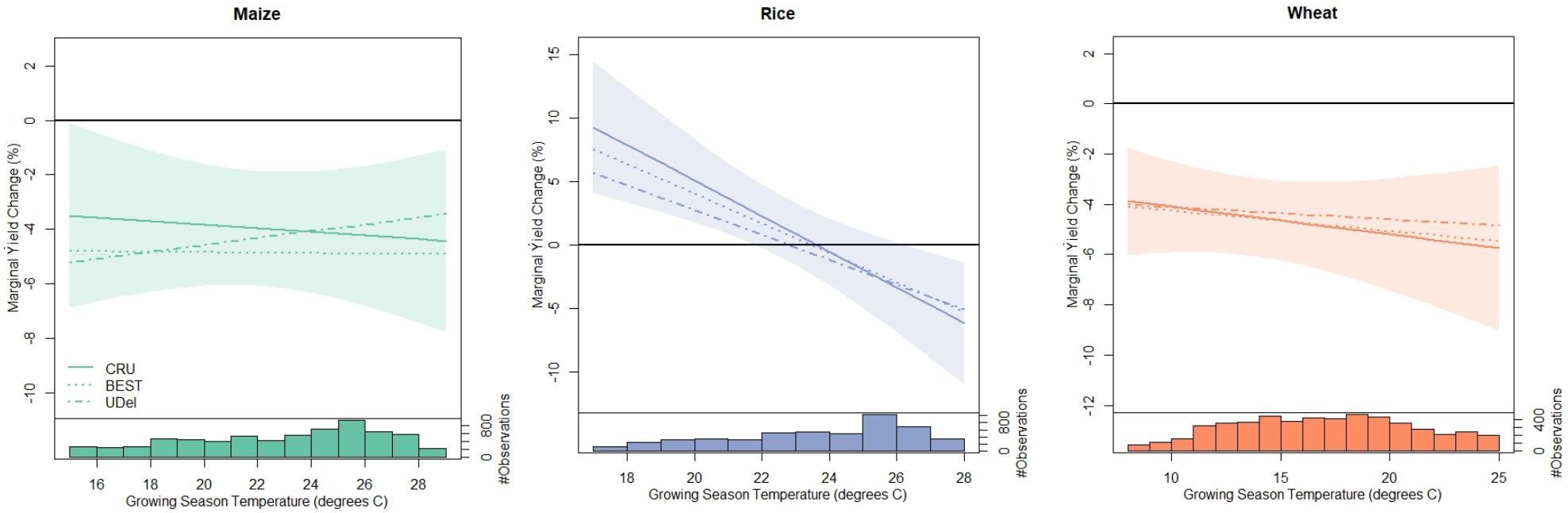

Figure Two: Sensitivity of Crop Yields to Warming. Effect of 1°C warming at different growing-season temperatures (marginal effect) estimated from the empirical crop model using three datasets for observed temperatures (Methods) for maize, rice and wheat. Values greater than zero indicate warming has a positive effect and less than zero indicate a negative effect. Shaded areas show the 95% confidence intervals using the CRU dataset, with residuals clustered at the country level to account for temporal autocorrelation and cross-crop correlations. Histograms show the distribution of observed growing season temperatures.

(17) estimate a one degree increase in temperature would reduce maize, wheat and rice yields by 7.4%, 6.0% and 3.2% respectively based on a large ensemble combining multiple process-based and empirical yield models. This compares to area-weighted average global effects of 4.0%, 4.8, and 4.2% yield reductions for maize, wheat and rice respectively estimated here. Given the uncertainty in both studies, these are statistically indistinguishable from each other. The estimated response is also robust to alternate observed temperature datasets (Figure 2). There are multiple pathways through which hot temperatures reduce yields, with several papers pointing to the important role of higher vapor-pressure deficit in driving evapo-transpiration that lowers available soil moisture late in the growing season (16, 49, 50). Other mechanisms include direct damage during the reproductive phase of the crop life-cycle and accelerated senescence that limits grain filling (51, 52).

Supplementary Figure 4 shows the estimated response to growing season precipitation. The effect is in the expected direction, with higher rainfall most beneficial in dry regions, providing declining benefits in wetter areas. The estimates are empirically fairly small compared to temperature: an increase of 10% in growing season rainfall, approximately double the mean observed absolute change in growing season precipitation since 1961, increases yields of maize, wheat, and rice by 1.4%, 0.4%, and 0.2% at the median. Except for maize, these are not statistically distinguishable from zero. These results follow previous findings in the literature, which has generally found trends in growing season rainfall to be not clearly distinguishable from zero and the empirical effects on crop yields to be small (25, 26, 49, 53).

In addition to controlling for observed growing-season rainfall, the empirical crop model controls for non-temperature drivers of yield through both country and crop-specific quadratic time trends that control for smooth, non-linear drivers of yield, and crop-year fixed-effects (dummy variables) that flexibly capture all crop-specific global yield shocks (Methods). Together, these account for the genetic progress in crop varieties, smooth increases in input use, and all other smoothly-varying or common global factors that might affect yields. Evidence for the effect of climate change is identified using deviations away from these time trends (additional discussion in Methods)

Figure 3a shows the change in yield between the first and last ten years of the sample (1961-1970 and 2008-2017) not explained by either the country-crop time trends or the crop-year fixed effects. The observed pattern shows a substantial slowing of yield growth, particularly for wheat and maize in parts of Africa and South America, as well as accelerations of rice yield growth in temperate parts of Europe, South America, and southern Africa, which have only small growing areas compared to the major rice producers in Asia. Figure 3a also shows the same measure of crop yield changes derived from two 500-

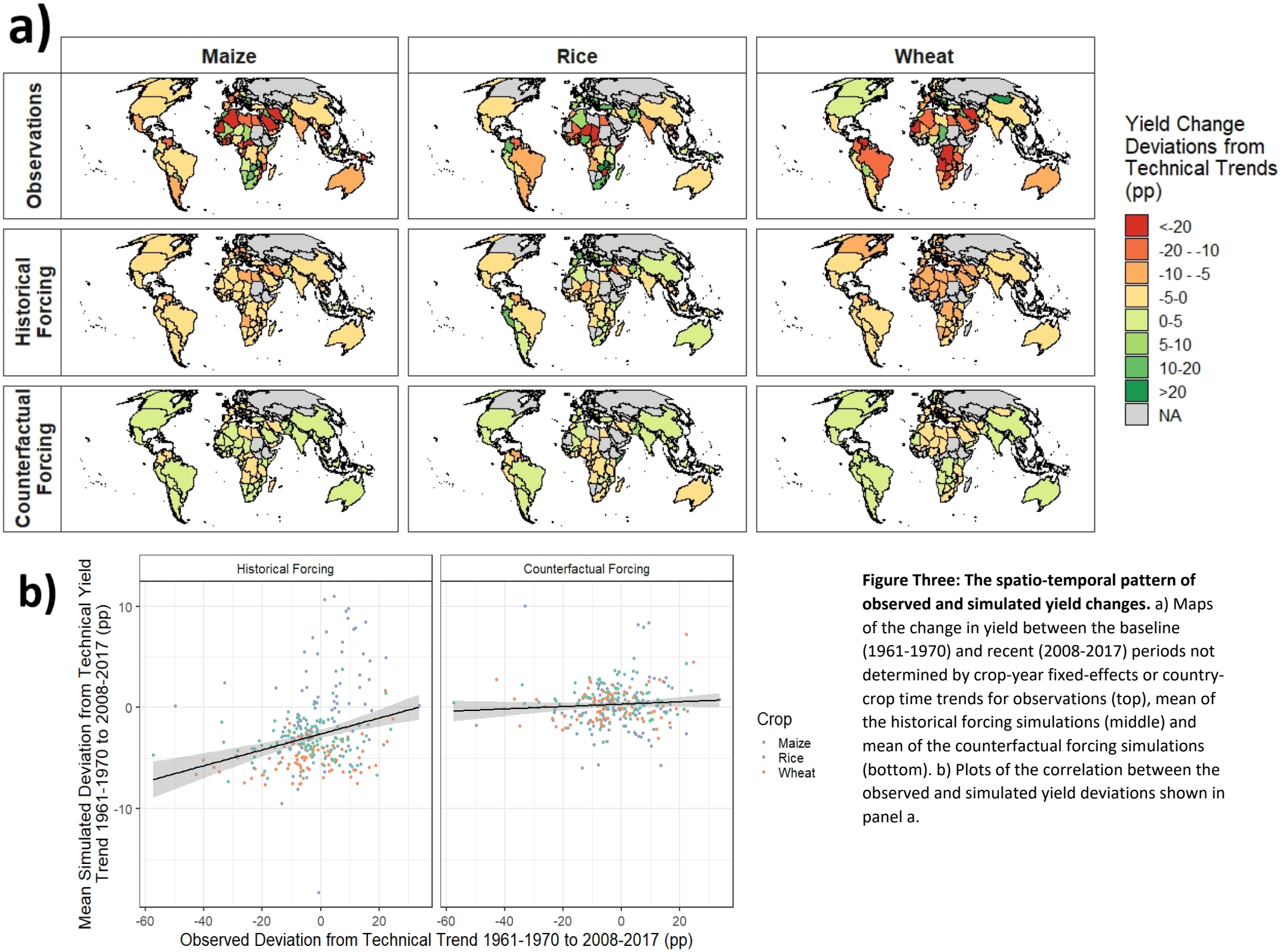

Figure Three: The spatio-temporal pattern of observed and simulated yield changes. a) Maps of the change in yield between the baseline (1961-1970) and recent (2008-2017) periods not determined by crop-year fixed-effects or country-crop time trends for observations (top), mean of the historical forcing simulations (middle) and mean of the counterfactual forcing simulations (bottom). b) Plots of the correlation between the observed and simulated yield deviations shown in panel a.

member yield ensembles generated by connecting the historical forcing and counterfactual forcing ensembles with the empirical yield model. These ensembles account for four sources of uncertainty: 1) internal climate variability (via the climate model ensemble), 2) the yield response to temperature change (by sampling the parameters of the yield model), 3) variance in non-temperature factors in the empirical yield model (by sampling parameter values), and 4) the variation in yield unexplained by the empirical model (by sampling the residual distribution of the yield model).

The historical forcing ensemble captures important characteristics of the observed pattern of yield growth since 1960, particularly slowing wheat yield growth over much of Africa and Europe and accelerating rice yields in cooler growing regions. These patterns are not apparent in the counterfactual forcing ensemble (Figure 3a). Figure 3b shows the correlation between observed yield changes and the ensemble means, confirming that simulations using historical forcing capture observed patterns across crops and countries ($p<0.0001$), while counterfactual simulations excluding greenhouse gas forcing do not ($p=0.2$).

While patterns from the ensemble means are suggestive, the variance resulting from convolving the range in the CESM ensemble with uncertainty in the parameters of the yield model is substantial. For any one crop-country combination, the probability of necessary and sufficient causation (PNS) does not exceed standard confidence levels (Supplementary Figure 5). The highest PNS of 79% is seen for positive effects of warming on Peruvian rice yields. However, although the signal of anthropogenic warming has not emerged strongly for any specific crop in any specific country, it is still possible that all 287 crop-country combinations in the sample show, in aggregate, the influence of anthropogenic warming.

In order to assess the aggregate global and multi-crop evidence for the influence of anthropogenic warming, I combine yield changes between the baseline and recent periods for all countries and crops into a single yield index. Index weighting is determined by the estimated signal-to-noise ratio of anthropogenic warming for that crop and country, in other words the magnitude of the warming signal divided by the empirical variance in the estimated signal defined using a training set of one third of the simulations (Methods). This weighting maximizes statistical power to detect the anthropogenic signal (45) since it accounts for the different response of crops to temperature change (i.e yield increases in some areas and decreases in other areas could both be consistent with the anthropogenic effect), variation in the exposure and sensitivity of crops to anthropogenic warming, and heterogeneity in the uncertainty of the estimated anthropogenic effect. The change in yield between a 1961-1970 start period and a 2008-2017 end period for each of the 287 crop-country combinations are aggregated into a one-dimensional index using this optimized weighting, shown in Supplementary Figure 6.

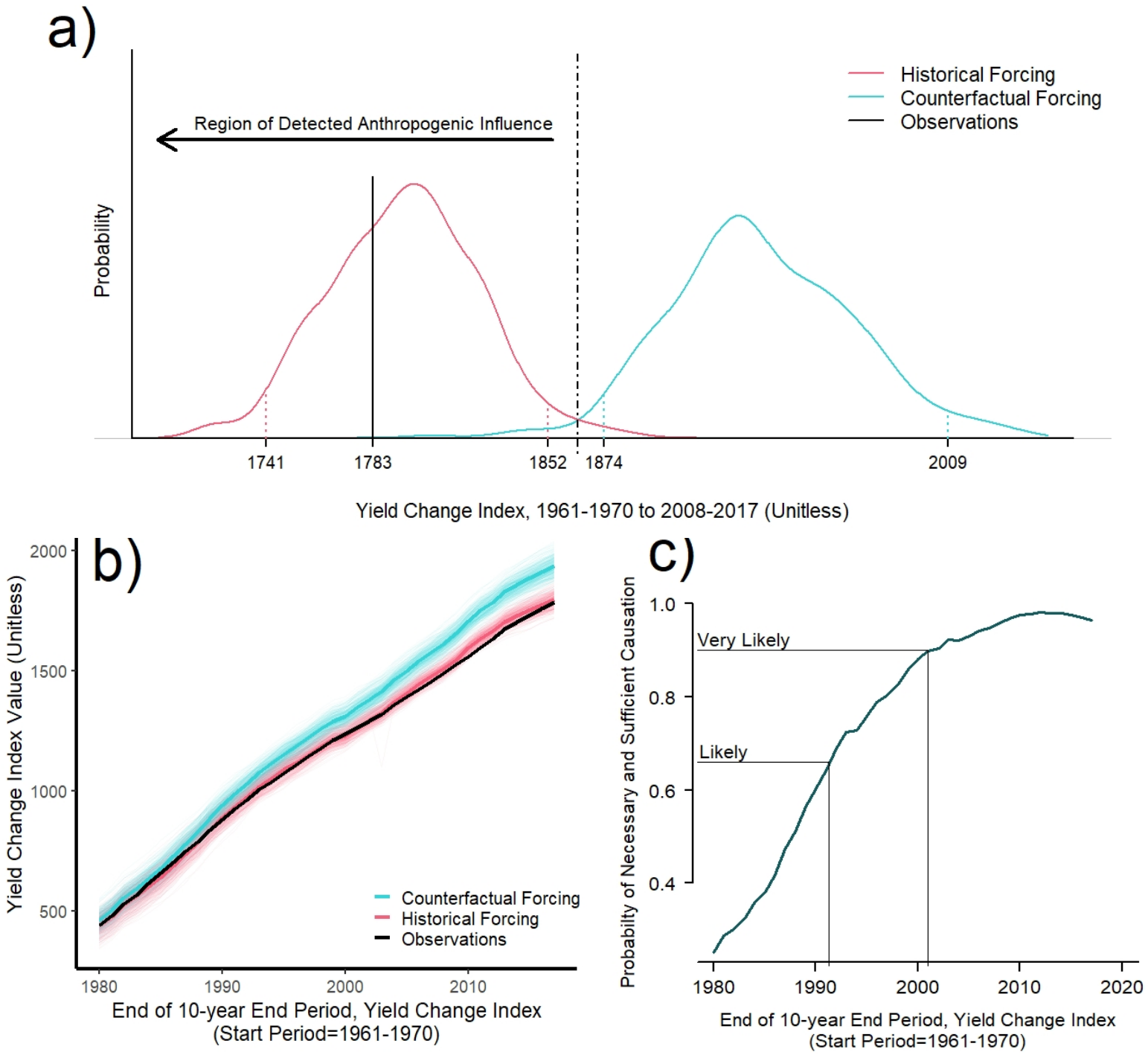

Figure Four: Identification and emergence of the signal of anthropogenic warming on global crop yields. a) Distribution of the global, multi-crop index of yield changes under historic and counterfactual forcing. Dashed line gives the threshold index value for a statistical test that maximizes the PNS. Observed values to the left of this threshold give evidence of a detected anthropogenic effect. Black line gives the observed value of the yield index, dotted lines give the quantiles defining the central 95% of the two distributions. b) Distributions of the index value over time using a rolling 10-year end-period showing the emergence of the anthropogenic warming signal. Each of the 335 simulations in the testing set of the historical and counterfactual forcing simulations is shown (thin lines) as well as the distribution means (thick lines) c) Separation of the index distributions under historical and counterfactual forcings, quantified using the probability of necessary and sufficient causation. Probabilities corresponding to “likely” (66%) and “very likely” (90%) are from Mastrandrea et al. (54)

Figure 4a shows the distribution of this global multi-crop yield change index under historical and counterfactual forcing for the 335 simulations excluded from the training set used to estimate index weights (Methods). The distributions are clearly well separated, with a maximum PNS of over 96%. A test to detect the anthropogenic signal divides possible index values into two regions - those consistent and those inconsistent with the influence of anthropogenic warming – with the threshold value chosen so as to maximize statistical power (dashed line, Figure 4a). Observed values of the yield change index are well within the region of detected anthropogenic influence, consistent with historic but not counterfactual forcing.

Figures 4b and 4c show the emergence of this anthropogenic warming signal over the end of the 20th century by calculating the yield change index between the 1961-1970 start period and a rolling 10-year end period ending between 1980 and 2017. The index values in Figure 4b show a large secular trend in all simulations, reflecting significant gains in yield over this time period due largely to improved technology and increasing inputs. This non-stationarity even in the absence of climate change has been identified previously as a major challenge to the detection and attribution of climate change impacts in human and managed systems generally (10). However, Figure 4b also shows the gradual separation of the two distributions over time, producing the well-separated distributions shown in Figure 4a by 2017.

Observed index values consistently track the historical forcing simulations and can not be explained by counterfactual forcings. Figure 4c quantifies the time of emergence of the anthropogenic warming signal showing the increasing separation of the two distributions, measured using PNS, over time. It is very likely (probability greater than 90%) that global crop yield growth since the early 2000s has been influenced by anthropogenic warming.

Because the identified signal of anthropogenic warming on crops includes both reductions in wheat yields and increases in rice yields in certain areas, the net effect on caloric production is ambiguous. I therefore quantify the effect of anthropogenic warming on global food security by aggregating the difference in agricultural production in the historic and counterfactual forcing simulations to the global level (Supplementary Figure 7a). The net effect on calorie production has been negative, dominated by wheat and maize, which are both more widely grown and more calorie dense than rice. In the 2008-2017 end-period, the central estimate is that warming from anthropogenic greenhouse gas emissions has reduced calorie production from wheat, rice, and maize, by 5.7%. Assuming a daily caloric requirement of 2,500 calories and allowing for 35% post-harvest losses (55), this is an amount sufficient to feed 315 million people.

The country-level calorie effect from anthropogenic warming is given in Supplementary Figure 7b. A consistent geographic signal is not strongly apparent due to counteracting effects from the sensitivity and exposure of crops to anthropogenic warming: crops in tropical areas are more sensitive to warming (Figure 2) but the magnitude of anthropogenic warming is larger in temperate countries (Figure 1a). Reductions of more than 10% in calorie production, relative to the case without anthropogenic warming, are apparent in parts of the Middle East and Central Asia (namely United Arab Emirates, Kazakhstan, Kuwait, and Oman). Net positive effects on calorie production are smaller and are limited to cooler rice-producing regions (particularly Japan and South Korea).

It is important to note that the yield impacts described here are those associated with the warming effect of greenhouse gas emissions, not with the effect of greenhouse gases themselves or with all radiatively-active anthropogenic emissions. Carbon dioxide has a directly beneficial effect on crops: a simple calculation based on a recent meta-analysis (27) suggests that CO_2 fertilization over the 1961-2017 period has raised yields of C_3 crops (rice and wheat) by 7.1% and of C_4 crops (maize) by 6.0%. These are more than enough to offset, at a global level, the negative effects of anthropogenic warming documented here. However, the effect of radiatively-active short-lived polluters such as aerosols and tropospheric ozone are also not considered. These affect crops through a number of pathways, including reducing the solar radiation available for photosynthesis, scattering incoming radiation, and direct ozone toxicity, in addition to their effects on local temperature (additional discussion in Methods) (34, 56). These effects are poorly constrained, but within certain regions, the negative effect is estimated to be much larger than benefits from CO_2 fertilization (34).

The influence of greenhouse gas emissions on the physical climate system is now well demonstrated (3, 4, 11) and a growing body of literature has documented the sensitivity of socio-economic outcomes to changes in climate (8, 9). However, directly detecting the signal of anthropogenic emissions on these outcomes is challenging because climate change may be only a small driver of change, and other key factors may be unobserved, unquantifiable, or poorly understood. Nevertheless, this analysis shows anthropogenic climate change has likely already had a discernable influence on global agricultural production. It is probable that continued global warming will lead to larger effects on agriculture as well as global emergence of the anthropogenic climate change signal in other economic sectors.

Methods

A schematic illustration of the method used in this paper is given in Supplementary Figure 2. Growing season temperature change under historical forcings (40 members) and the counterfactual forcing that omits greenhouse gas emissions since 1920 (20 members) are from two large ensembles of the CESM model (40). Although many detection and attribution studies have compared the effect of historical to natural forcings, netting out the effect of aerosol cooling from greenhouse gas warming, this would greatly complicate the yield analysis. Aerosols affect crops not only via growing season temperature but also by changing the sunlight available for photosynthesis and by altering the scatter of incoming radiation (56, 57). This effect is not empirically well constrained on a global scale and varies by aerosol species (57), meaning including the aerosol effect would add substantial uncertainty to the yield response modeling. Tropospheric ozone is similarly complex in that, in addition to its effect on climate, it is also directly toxic to crops. The yield effects of ozone and aerosols through these 'non-climate' pathways is likely much larger than their effect on crops via changes in temperature (57). Accordingly this paper focuses only on the causal effect of radiative forcing from greenhouse gas emissions using the CESM ensembles.

Since the CESM is the only model to run these leave-one-out detection and attribution ensembles, climate model uncertainty is not sampled in the analysis. Supplementary Figure 8a provides a comparison between observed terrestrial temperature change since 1960, the LENS distribution, and the CMIP5 inter-model spread (58). Natural variability captured by the LENS overlaps with a large majority (lower 75%) of the CMIP5 distribution. The upper 25th percentile of the CMIP5 distribution simulates rapid warming since 1990 that is outside the LENS distribution. But this upper tail is also substantially larger than warming in the observational record. Supplementary Figure 8b compares the LENS distribution to observed country-crop-level changes in growing-season temperature over growing-areas. While there is no evidence of systematic bias in the LENS warming rates, there is evidence that the range of observations is wider than captured by the LENS. This could be consistent either with noise in observational data or an under-sampling of natural variability by CESM.

Comparison to both observations and the CMIP5 distribution therefore suggests it is possible that reliance on a large ensemble from a single model may somewhat understate the true variance in temperature change, leading to overconfidence in identification of the anthropogenic signal. However, this effect is unlikely to substantively affect the main conclusions of the study for two reasons. Firstly, the LENS distribution is missing only the highest 25th percentile of warming from the CMIP5 ensemble. This means that expanding the temperature distribution to account for the models at the high-end of

the CMIP 5 distribution would likely increase the estimate of the anthropogenic warming signal, since these models appear to display a higher sensitivity to anthropogenic forcing. This would lead to a larger estimated effect on crop yields and greater confidence in the detection result. Secondly, temperature variability is a relatively small driver of variance in the simulated index values. The distribution of index values under historical forcing using only LENS temperature variability, ignoring parameter or residual uncertainty, reduces variance by 79%, implying the empirical yield model accounts for the large majority of index variance. Therefore, it is unlikely that a small expansion of the distribution of temperature changes, consistent with observations or the CMIP5 inter-model spread, would overturn evidence for the anthropogenic signal.

National yield data for maize, wheat, and rice from 1961-2017 from the Food and Agriculture Organization (FAO) (59) is used for the empirical yield model. Although national-level FAO data are known to contain measurement error, it is the only source of global, multi-crop yield data over a time-span long enough to identify the emergence of a climate change signal. To the extent FAO yield data is noisy, this will increase standard errors and residual variance, but will not bias estimates of the temperature effect on yield (60). Because both uncertainty in the yield response function and residual variance are sampled in the detection and attribution analysis, this will tend to increase the variance of the index distributions, leading to more overlap between the historical and counterfactual distributions and therefore a more conservative detection and attribution finding.

Yield data is merged with observations of temperature and precipitation from the Climate Research Unit, aggregated as described above using growing-season dates and growing areas (41, 61, 62). For winter wheat, the growing season is taken to be the four months prior to harvest date. To check robustness to alternate observational datasets, the yield model is also estimated using the Berkeley Earth temperature dataset (with CRU precipitation data) (63), and the University of Delaware temperature and rainfall datasets (64, 65). Growing area data and the calorie density of wheat, rice, and maize are also taken from the FAO (59).

An empirical model of yields is specified as follows, similar to the specification in Lobell et al. (25):

$$\log(y_{ict}) = \beta_{1c}T_{ict}I_c + \beta_{2c}{T_{ict}}^2I_c + \beta_{3c}P_{ict}I_c + \beta_{4c}{P_{ict}}^2I_c + \beta_{5ic}tI_{ic} + \beta_{6ic}t^2I_{ic} + \theta_{ic} + \vartheta_{ct} + \varepsilon_{ict} \quad (1)$$

Where y_{ict} is the yield of crop c in country i in year t, $\beta_{1c}T_{ict}I_c + \beta_{2c}{T_{ict}}^2I_c$ are crop-specific quadratics in growing-season temperature and $\beta_{3c}P_{ict}I_c + \beta_{4c}{P_{ict}}^2I_c$ are the same in growing-season precipitation. The $\beta_{5ic}tI_{ic} + \beta_{6ic}t^2I_{ic}$ terms are crop*country specific quadratic time trends, which capture smoothly trending, unobserved, country-crop specific factors affecting yield such as

technological progress. θ_{ic} is a set of country-crop specific fixed-effect (dummy variables) capturing all time-invariant differences between crop yields and ϑ_{ct} is a set of year-crop fixed-effects capturing all changes in yield that are common across countries.

For regression stability, temperature and precipitation are normalized prior to estimation. In addition, only country-crop combinations with at least 15 years of data are included. This gives 355 country-crop combinations and a total of 18155 observations. Estimation is done using Ordinary Least Squares (OLS) with standard errors clustered at the country level, allowing for arbitrary correlation of residuals across years and crops within a country. The regression model in total explains 92.8% of the variance in the dependent variable (R^2=0.928).

Since a large part of the anthropogenic warming signal is either global or smoothly changing at the country level, this variation is captured in the year-crop fixed effects (ϑ_{ct}) and the country-crop quadratic time trends ($\beta_{5ic}tI_{ic} + \beta_{6ic}t^2I_{ic}$). Parameters of the yield-temperature response function ($\beta_{1c}T_{ict}I_c + \beta_{2c}{T_{ict}}^2I_c$) are estimated using residual variation in country-level growing-season temperature after controlling for these global changes and smooth time trends. This principally reflects inter-annual weather variability (see illustration for French wheat temperatures in Supplementary Figure 9). This residual weather variation used to estimate the response function parameters is quasi-random and therefore highly unlikely to be correlated with other factors affecting yield (66). To the extent the parameters of the yield-temperature response, the year-crop fixed effects, and the country-level time trends are co-determined due to long-term, smooth temperature trends, this will be captured as the covariance between parameters of the yield model and accounted for in the uncertainty sampling scheme used to produce the historical and counterfactual yield distributions in Figure 4.

A distribution of 500 possible alternate yield trajectories over the 1961-2017 period for each of the 355 country-crop combinations under both historical and counterfactual forcings is generated. These distributions reflect three sources of uncertainty: natural variability captured by the CESM ensemble, uncertainty in the parameters of the empirical yield model, and the variance in yields not explained by the yield model, captured by the residual variation. For each simulation, I first sample growing season temperatures uniformly from the historic and counterfactual ensemble, then estimate predicted yields by combining sampled growing season temperatures with a draw from the estimated multivariate distribution of parameters of the yield model, and finally simulate yields by adding a draw from the residual distribution.

A training set of one third of the simulations (n=165) is randomly drawn from the simulations. This is used to calculate the optimal weighting of the global yield change index. Weightings in the index are given by:

$$W_{ict} = \frac{\bar{\Delta}y_{1ic} - \bar{\Delta}y_{0ic}}{Var(\Delta y_{0ic})}$$

Where $\bar{\Delta}y_{1ic}$ is the mean change in yield of crop c in country i in the historical forcing simulations between the initial 10 years of the sample (1961-1970) and the final 10 years (2008-2017) in the training set and $\bar{\Delta}y_{0ic}$ is the same for the counterfactual forcing simulations (i.e. the signal of greenhouse gas emissions on yield growth). The denominator is the estimated variance of yield changes in the counterfactual simulations. Because some countries are missing data for the start period, the number of crop-country combinations drops to 287 for this analysis.

The remaining two thirds (n=335) simulations are aggregated to a single index using the weightings derived from the training set to produce distributions of the index under historical and counterfactual forcings. The observed value of the yield index is calculated using the same weightings applied to observed yield changes. The threshold value for the index, defining the region of identified anthropogenic influence, is chosen as the value that maximizes the probability of necessary and sufficient causation, which is the point of maximum separation of the CDF of the two distributions. For Figures 4b and 4c, the yield change index is calculated for each simulation using a rolling 10-year end period ending in each year from 1980 to 2017.

The estimated effect of anthropogenic warming on global calorie production from wheat, rice, and maize is calculated as:

$$\Delta Cal_t = \sum_{ic} A_{ict} k_c \, \Delta\hat{y}_{ict}$$

Where A_{ict} is the area of crop c in country i in year t and k_c is the calorie density of crop c. $\Delta\hat{y}_{ict}$ is the estimated change in yield due to anthropogenic warming. Uncertainty sampling in Supplementary Figure 7a uses a ceteris paribus assumption that is standard to the climate impacts literature, but is relaxed for the detection and attribution analysis shown in Figure 4. Uncertainty sampling reflects natural variability in temperature (from sampling the CESM ensembles) and uncertainty in the yield response to temperature (from sampling the parameters of the temperature response function, β_{1c} and β_{2c} in Equation 1).

References

1. B. D. Santer, *et al.*, Identifying human influences on atmospheric temperature. *Proc. Natl. Acad. Sci. U. S. A.* **110**, 26–33 (2013).

2. T. P. Barnett, *et al.*, Penetration of human-induced warming into the world's oceans. *Science (80-.).* **309**, 284–287 (2005).

3. X. Zhang, *et al.*, Detection of human influence on twentieth-century precipitation trends. *Nature* **448**, 461–5 (2007).

4. K. Marvel, C. Bonfils, Identifying External Influences on Global Precipitation. *Proc. Natl. Acad. Sci.* **110**, 19301–19306 (2013).

5. S. Min, X. Zhang, F. W. Zwiers, G. C. Hegerl, Human Contribution to More-Intense Precipitation Extremes. *Nature* **470**, 378–381 (2011).

6. T. P. Barnett, *et al.*, Human-induced changes in the hydrology of the western United States. *Science (80-.).* **319**, 1080–1083 (2008).

7. C. C. Hay, *et al.*, On the Robustness of Bayesian Fingerprinting Estimates of Global Sea Level Change. *J. Clim.* **30**, 3025–3038 (2017).

8. T. A. Carleton, S. M. Hsiang, Social and economic impacts of climate. *Science (80-.).* **353**, 1112 (2016).

9. M. Dell, B. F. Jones, B. A. Olken, What Do We Learn from the Weather? The New Climate-Economy Literature. *J. Econ. Lit.* (2014).

10. D. Stone, *et al.*, The challenge to detect and attribute effects of climate change on human and natural systems. *Clim. Change* **121**, 381–395 (2013).

11. B. D. Santer, *et al.*, A Search for Human Influence on the Thermal Structure of the Atmosphere. *Nature* **382**, 39–46 (1996).

12. M. Dell, B. F. Jones, B. A. Olken, Temperature Shocks and Economic Growth: Evidence from the Last Half Century. *Am. Econ. J. Macroecon.* **4**, 66–95 (2012).

13. K. J. Mach, *et al.*, Climate as a risk factor for armed conflict. *Nature* **571**, 193–197 (2019).

14. O. Deschênes, M. Greenstone, Climate Change, Mortality, and Adaptation: Evidence from Annual Fluctuations in Weather in the US. *Am. Econ. J. Appl. Econ.* **3**, 152–185 (2011).

15. W. Cramer, *et al.*, "Chapter 18: Detection and Attribution" in *Climate Change 2014: Impacts, Adaptation and Vulnerability. Working Group 2 Contribution to the IPCC 5th Assessment Report*, (Cambridge University Press, 2014).

16. D. B. Lobell, *et al.*, The Critical Role of Extreme Heat for Maize Production in the United States. *Nat. Clim. Chang.* **3**, 497–501 (2013).

17. B. Liu, *et al.*, Similar estimates of temperature impacts on global wheat yield by three independent methods. *Nat. Clim. Chang.* **6**, 1130–1136 (2016).

18. C. Zhao, *et al.*, Temperature increase reduces global yields of major crops in four independent estimates. *Proc. Natl. Acad. Sci.* **114**, 9326–9331 (2017).

19. J. R. Porter, *et al.*, "Chapter 7: Food Security and Food Production Systems" in *Climate Change*

2014: Impacts, Adaptation and Vulnerability. Working Group 2 Contribution to the IPCC 5th Assessment Report, (Cambridge University Press, 2014).

20. FAO, *Climate Change and Food Systems: Global Assessments and Implications for Food Security and Trade*, A. Elbehri, Ed. (Food and Agriculture Organization, 2015).

21. M. Lin, P. Huybers, Reckoning Wheat Yield Trends. *Environ. Res. Lett.* **7**, 024016 (2012).

22. P. Grassini, K. M. Eskridge, K. G. Cassman, Distinguishing Between Yield Advances and Yield Plateaus in Historical Crop Production Trends. *Nat. Commun.* **4**, 2918 (2013).

23. D. Ray, N. Ramankutty, N. Mueller, P. West, J. Foley, Recent patterns of crop yield growth, stagnation, and collapse. *Nat. Commun.* **3** (2012).

24. D. B. Lobell, The Case of the Missing Wheat. *Environ. Res. Lett.* **7**, 024016 (2012).

25. D. B. Lobell, W. Schlenker, J. Costa-Roberts, Climate Trends and Global Crop Production Since 1980. *Science (80-.).* **333**, 616–620 (2011).

26. W. Schlenker, D. L. Roberts, Nonlinear Temperature Effects Indicate Severe Damages to U.S. Corn Yields Under Climate Change. *Proc. Natl. Acad. Sci.* **106**, 15594–15598 (2009).

27. F. C. Moore, U. Baldos, T. W. Hertel, D. Diaz, New Science of Climate Change Impacts on Agriculture Implies Higher Social Cost of Carbon. *Nat. Commun.* **8**, 1601 (2017).

28. E. Hawkins, R. Sutton, The Potential to Narrow Uncertainty in Regional Climate Predictions. *Bull. Am. Meteorol. Soc.* **90**, 1095–1107 (2009).

29. C. Deser, R. Knutti, S. Solomon, A. S. Phillips, Communication of the Role of Natural Variability in Future North American Climate. *Nat. Clim. Chang.* **2**, 775–780 (2012).

30. S. Sippel, N. Meinshausen, E. M. Fischer, E. Székely, R. Knutti, Climate change now detectable from any single day of weather at global scale. *Nat. Clim. Chang.* **10**, 35–41 (2020).

31. G. Hansen, D. Stone, Assessing the observed impact of anthropogenic climate change. *Nat. Clim. Chang.* **6**, 532–9 (2016).

32. I. Supit, *et al.*, Recent Changes in the Climatic Yield Potential of Various Crops in Europe. *Agric. Syst.* **103**, 683–694 (2010).

33. D. K. Ray, *et al.*, Climate change has likely already affected global food production. *PLoS One* **14**, e0217148 (2019).

34. J. Burney, V. Ramanathan, Recent climate and air pollution impacts on Indian agriculture. *Proc. Natl. Acad. Sci. U. S. A.* **111**, 16319–24 (2014).

35. F. Tao, D. Xiao, S. Zhang, Z. Zhang, R. P. Rotter, Wheat yield benefited from increases in minimum temperature in the Huang-Huai-Hai Plain of China in the past three decades. *Agric. For. Meteorol.* **239**, 1–14 (2017).

36. F. Tao, *et al.*, Historical Data Provide New Insight Into Response and Adaptation of Maize Production Systems to Climate Change/Variabilty in China. *F. Crop. Res.* **185**, 1–11 (2016).

37. T. Palosuo, *et al.*, Effects of Climate and Historical Adaptation Measures on Barley Yield Trends in Finland. *Clim. Res.* **65**, 221–236 (2015).

38. F. C. Moore, D. B. Lobell, The Fingerprint of Climate Trends on European Crop Yields. *Proc. Natl.*

Acad. Sci. **11**, 2670–2675 (2015).

39. N. Brisson, *et al.*, Why are Wheat Yields Stagnating in Europe? A Comprehensive Data Analysis for France. *F. Crop. Res.* **119**, 201–212 (2010).

40. J. E. Kay, *et al.*, The Community Earth System Model (CESM) Large Ensemble Project: A Community Resource for Studying Climate Change in the Presence of Internal Climate Variability. *Bull. Am. Meteorol. Soc.* **96**, 1333–1349 (2013).

41. C. Monfreda, N. Ramankutty, J. A. Foley, Farming the planet: 2. Geographic distribution of crop areas, yields, physiological types, and net primary production in the year 2000. *Global Biogeochem. Cycles* **22**, n/a-n/a (2008).

42. I. Harris, T. J. Osborn, P. Jones, D. Lister, Version 4 of the CRU TS Monthly High-Resolution Gridded Multivariate Climate Dataset. *2Scientific Data* **7**, 109 (2020).

43. K. E. Kunkel, *et al.*, Can CGCMs Simulate the Twentieth-Century "Warming Hole" in the Central United States? *J. Clim.* **19**, 4137–4153 (2006).

44. N. D. Mueller, *et al.*, Cooling of US Midwest summer temperature extremes from cropland intensification. *Nat. Clim. Chang.* **6**, 317–322 (2016).

45. A. Hannart, P. Naveau, Probabilities of Causation of Climate Change. *J. Clim.* **31**, 5507–5524 (2018).

46. A. Hannart, *et al.*, Causal Counterfactual Theory for the Attribution of Weather and Climate-Related Events. *Bull. Am. Meteorol. Soc.* **97**, 99–110 (2016).

47. K. A. McKinnon, C. Deser, Internal Variability and Regional Climate Trends in an Observational Large Ensemble. *J. Clim.* **31**, 6783–6802 (2018).

48. C. Rosenzweig, *et al.*, Assessing agricultural risks of climate change in the 21st century in a global gridded crop model intercomparison. *Proc. Natl. Acad. Sci. U. S. A.* **111**, 3268–73 (2014).

49. A. Ortiz-Bobea, H. Wang, C. M. Carrillo, T. R. Ault, Unpacking the climatic drivers of US agricultural yields. *Environ. Res. Lett.* **14**, 064003 (2019).

50. D. B. Lobell, *et al.*, Greater sensitivity to drought accompanies maize yield increase in the U.S. Midwest. *Science* **344**, 516–9 (2014).

51. D. B. Lobell, A. Sibley, J. Ivan Ortiz-Monasterio, Extreme heat effects on wheat senescence in India. *Nat. Clim. Chang.* **2**, 186–189 (2012).

52. J. L. Hatfield, J. H. Prueger, Temperature extremes: Effect on plant growth and development. *Weather Clim. Extrem.* **10**, 4–10 (2015).

53. W. Schlenker, D. B. Lobell, Robust negative impacts of climate change on African agriculture. *Environ. Res. Lett.* **5**, 014010 (2010).

54. M. D. Mastrandrea, *et al.*, "Guidance Note for Lead Authors of the IPCC Fifth Assessment Report on the Consistent Treatment of Uncertainties" (2010).

55. P. Alexander, *et al.*, Losses, inefficiencies and waste in the global food system. *Agric. Syst.* **153**, 190 (2017).

56. J. Proctor, S. Hsiang, J. Burney, M. Burke, W. Schlenker, Estimating global agricultural effects of geoengineering using volcanic eruptions. *Nature* **560**, 480–483 (2018).

57. J. Burney, V. Ramanathan, Recent climate and air pollution impacts on Indian agriculture. *Proc. Natl. Acad. Sci. U. S. A.* **111**, 16319–24 (2014).

58. K. E. Taylor, R. J. Stouffer, G. A. Meehl, An Overview of CMIP5 and the Experiment Design. *Bull. Am. Meteorol. Soc.* **93**, 485–498 (2012).

59. FAO, FAOSTAT, V.3 (2016) (April 4, 2016).

60. J. Angrist, J. S. Pischke, *Mostly Harmless Econometrics* (Princeton University Press, 2009).

61. I. Harris, P. D. Jones, T. J. Osborn, D. H. Lister, Updated high-resolution grids of monthly climatic observations - the CRU TS3.10 Dataset. *Int. J. Climatol.* **34**, 623–642 (2014).

62. W. J. Sacks, D. Deryng, J. A. Foley, N. Ramankutty, Crop Planting Dates: An Analysis of Global Patterns. *Glob. Ecol. Biogeogr.* **19**, 607–620 (2010).

63. BEST, Berkeley Earth Data (2018) (March 5, 2018).

64. K. Matsuura, Willmott, Terrestrial Air Temperature: 1900-2017 Gridded Monthly Time Series Version 5.01 (2018).

65. K. Matsuura, C. J. Willmott, Terrestrial Precipitation: 1900-2017 Gridded Monthly Time Series Version 5.01 (2018).

66. O. Deschênes, M. Greenstone, The Economic Impacts of Climate Change: Evidence from Agricultural Output and Random Fluctuations in Weather. *Am. Econ. Rev.* **97**, 354–385 (2007).

Acknowledgements

The work described here benefited enormously from the intellectual contribution of Alexis Hannart who developed the weighting scheme for the optimal crop yield change index. It was supported by USDA NIFA (Award # 12225279).

Supplementary Information

a)

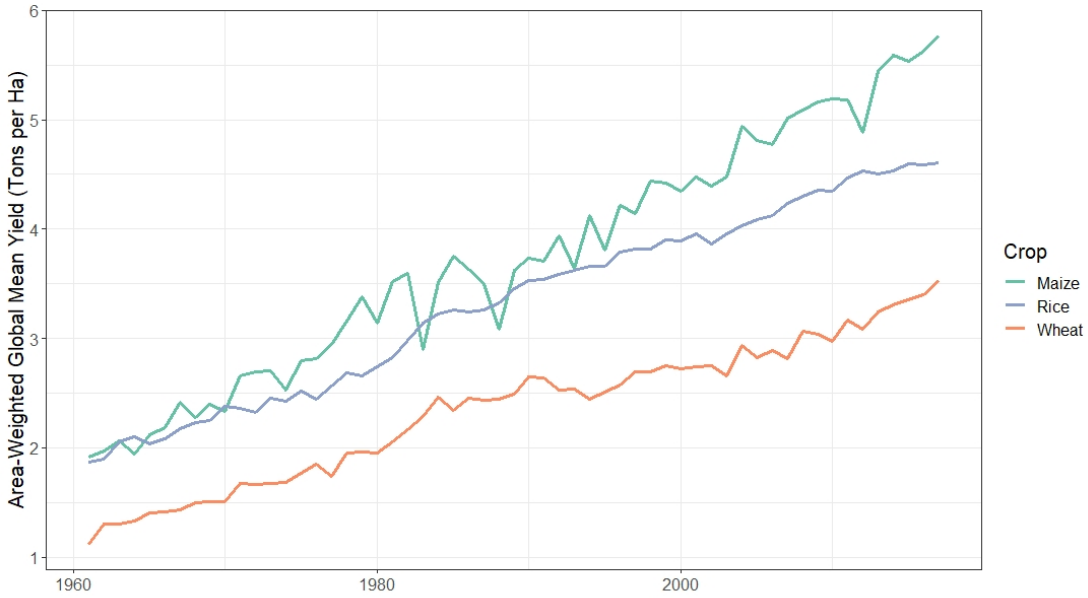

b)

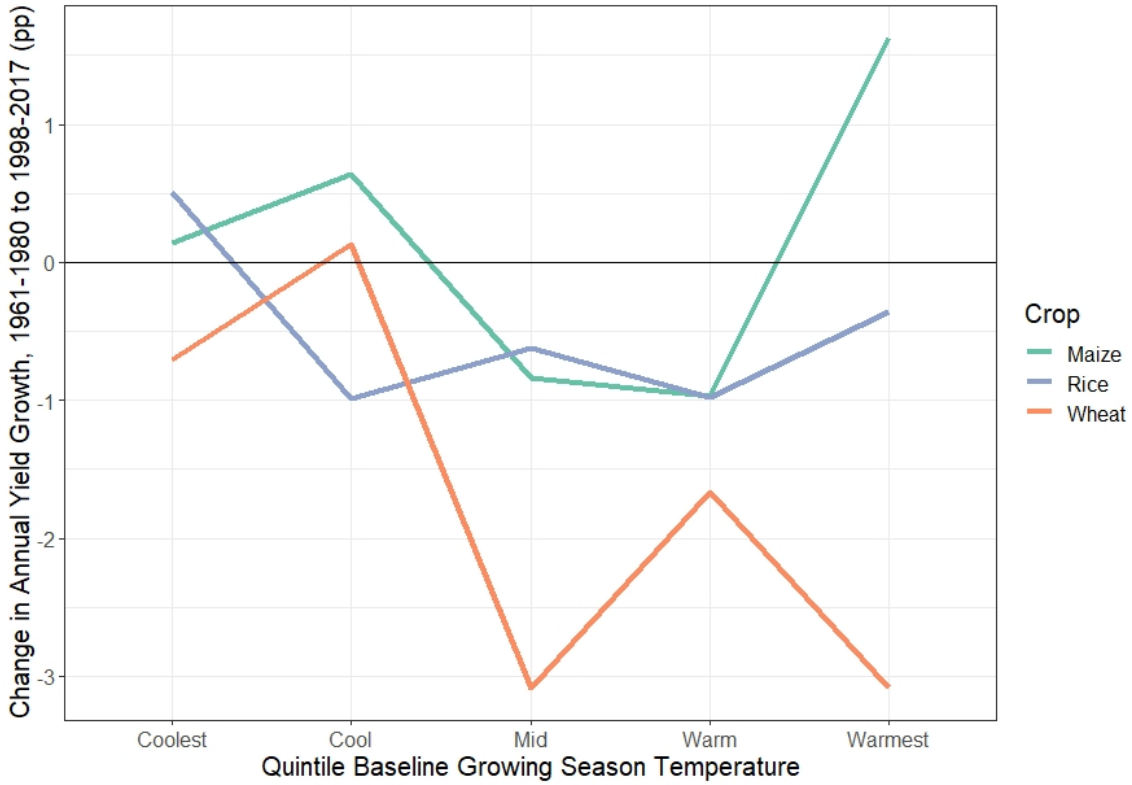

Supplementary Figure 1: a) Global observed, area-weighted yields over the sample period, 1961-2017. b) Observed change in yield growth by crop and distribution of baseline (pre-1981) growing-season temperatures between the first 20 years in the sample (1961-1980) and the last 20 years (1998-2017) in percentage points (pp).

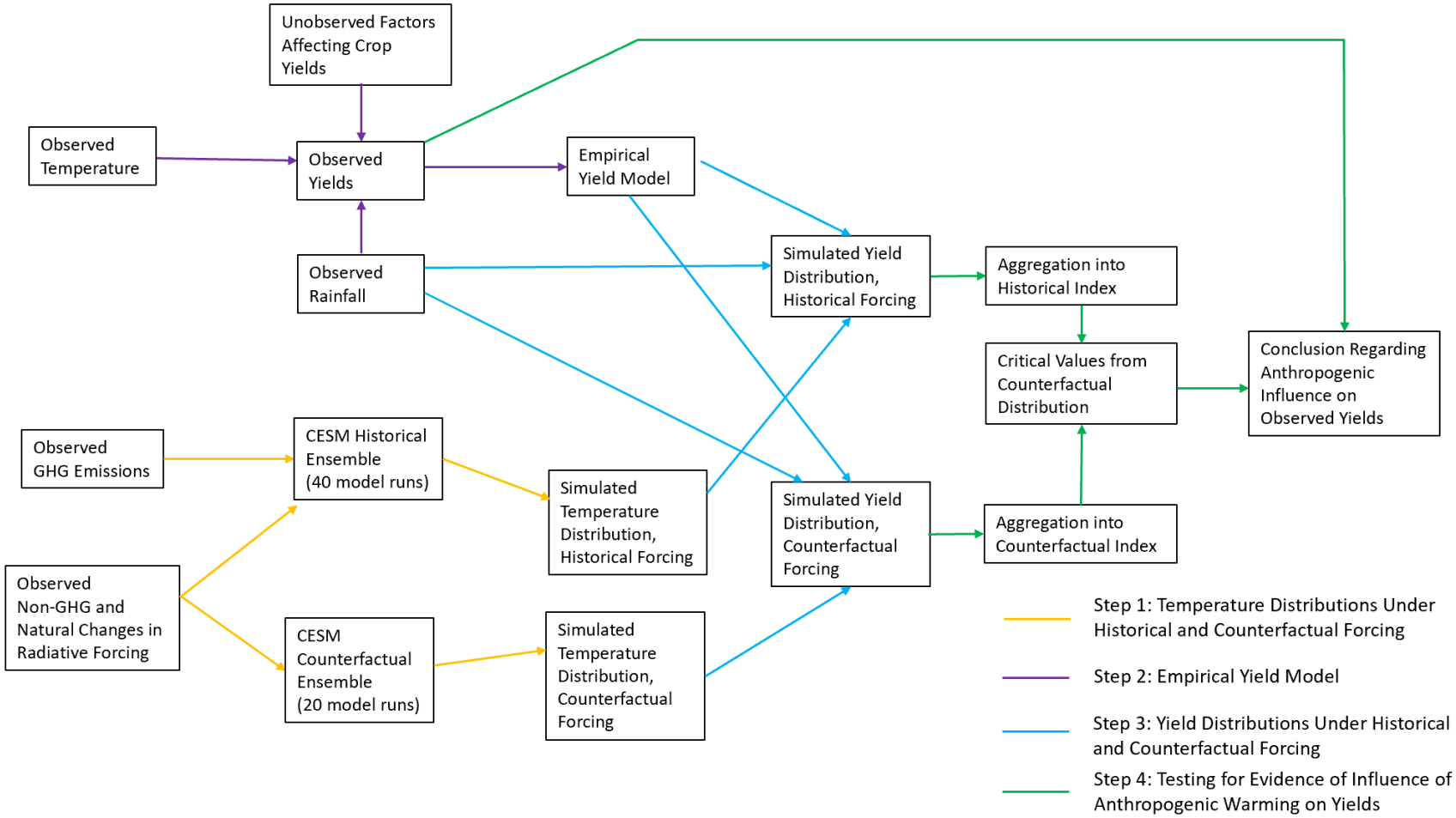

Supplementary Figure 2: Schematic diagram of methodological approach in this paper

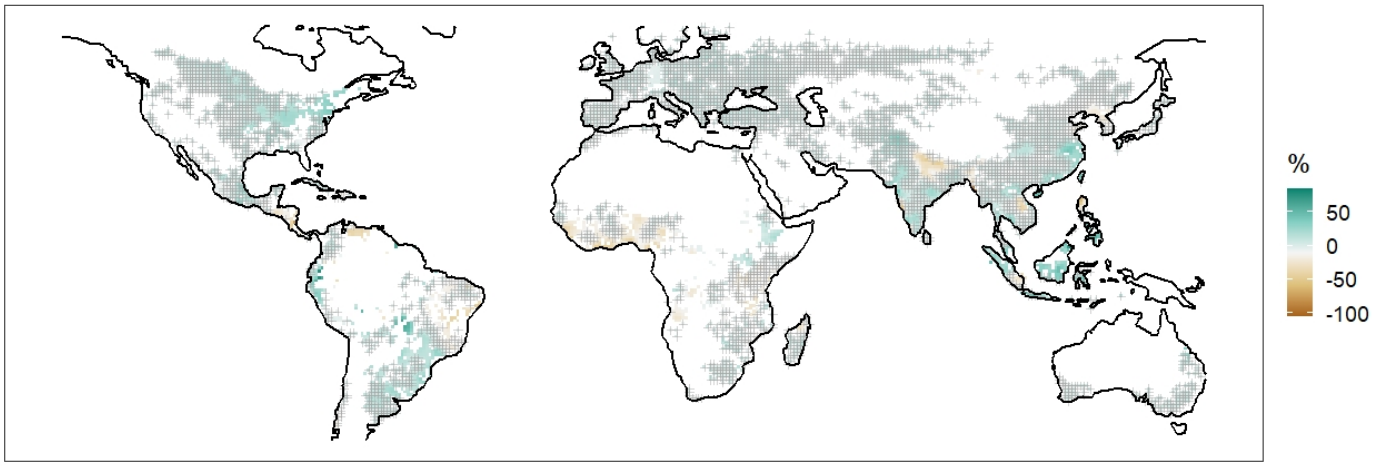

Supplementary Figure 3: Observed change in growing season rainfall over wheat, rice and maize growing areas (grid cells with >50 Ha combined in 2000 (41)) between 1961-1970 and 2008-2017 (42), given as % change relative to baseline period. Growing-season trends for the three crops are a calorie-weighted average of production for each grid cell. Grey crosses indicate areas where the observed change is within the central 95% of the distribution from the counterfactual climate model ensemble that omits greenhouse gas emissions since 1920.

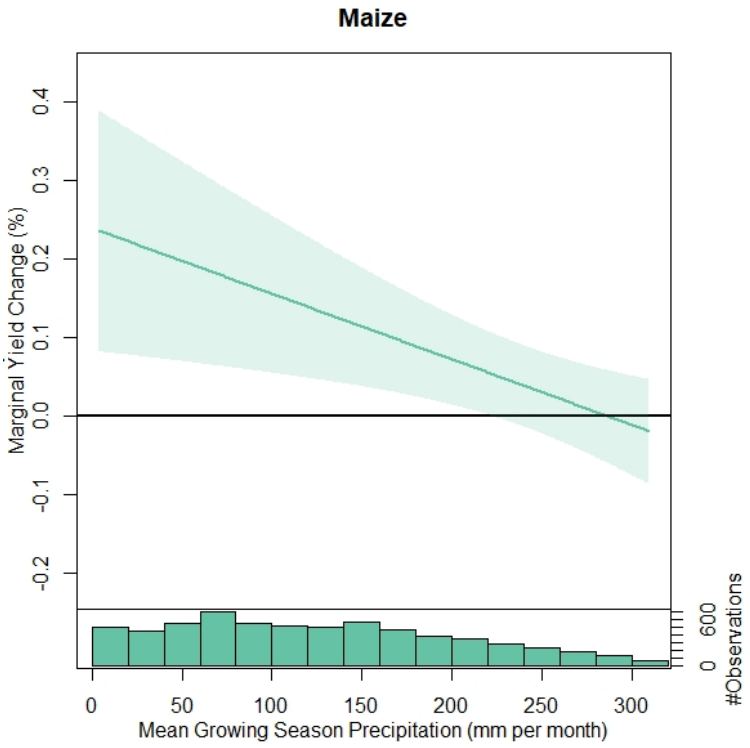

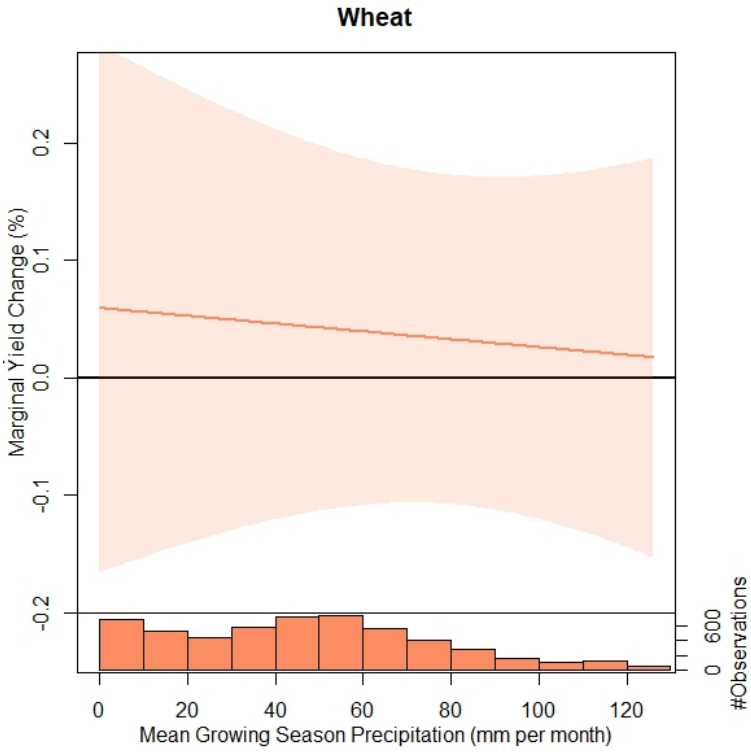

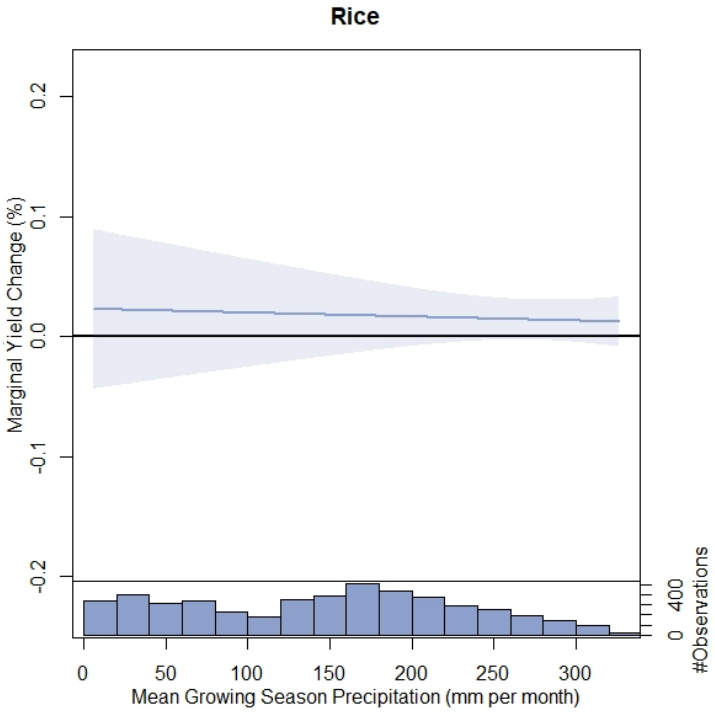

Supplementary Figure 4: Estimated marginal response of yields to growing-season rainfall in (mm per month) for maize, rice, and wheat. The straight lines are the gradients of the quadratic response functions estimated using Equation 1 (Methods). Values above the x-axis correspond to a positive response to increased rainfall.

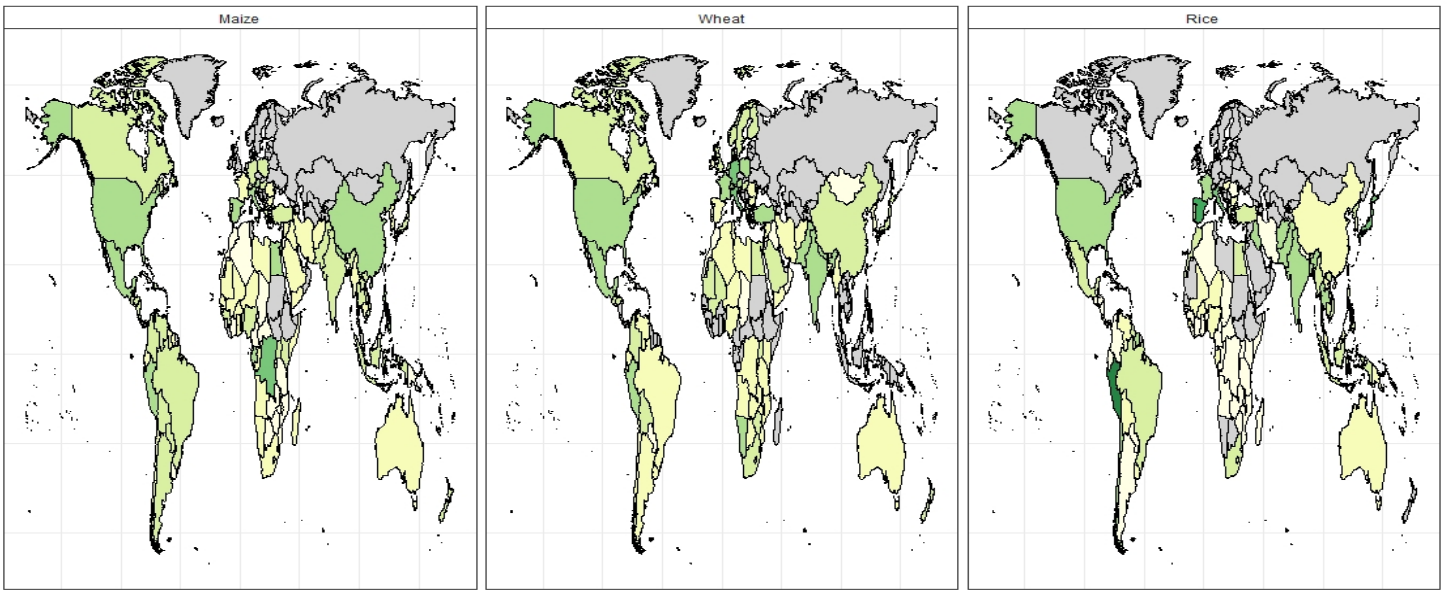

Supplementary Figure 5: Probability of necessary and sufficient causation (PNS) by crop and country. PNS measures the separation of the distribution of yield changes under historical and counterfactual forcing and is the maximum separation of the two cumulative distribution functions(46). PNS in this context can also be interpreted as the one minus the combined probability of a false negative and a false positive given a threshold for the test statistic designed to maximize PNS.

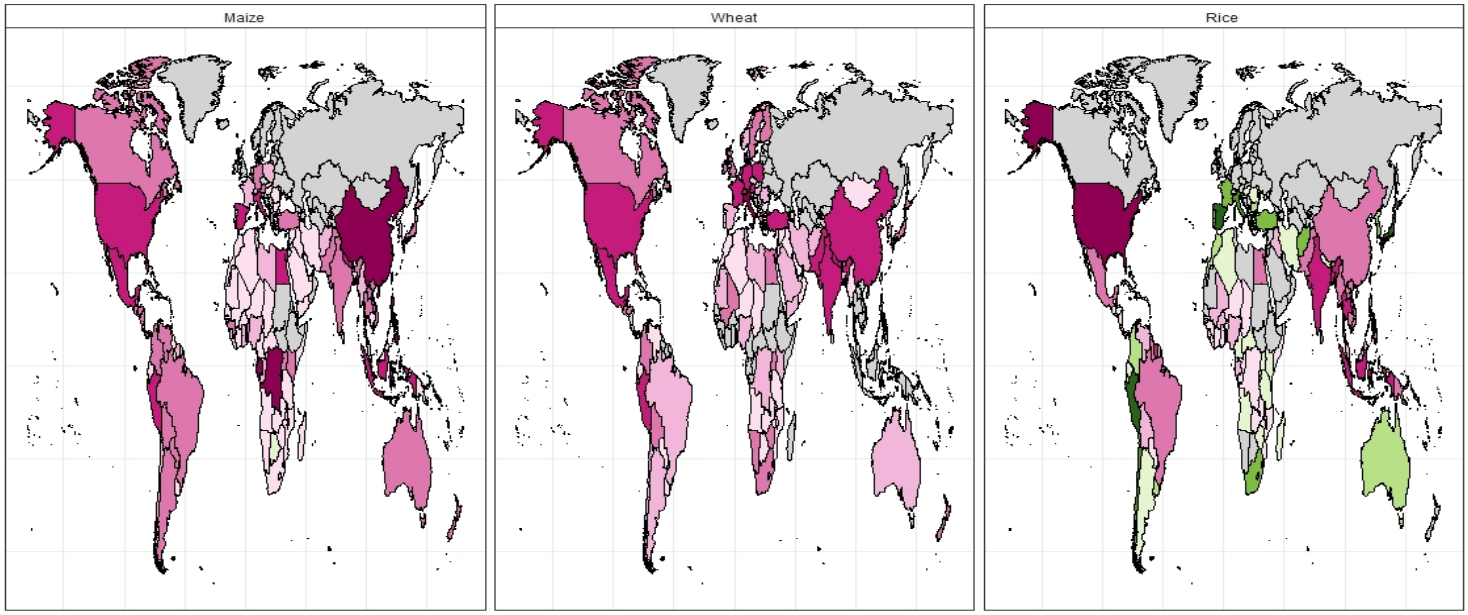

Supplementary Figure 6: Weightings by crop and country in the yield growth signal-to-noise index. Weighting is based on the estimated signal to noise ratio of the anthropogenic effect of crop yields (Methods). The index is also directional (i.e. takes positive and negative values), accounting for the fact that the same warming signal might have opposite effects on yield depending on the crop and location.

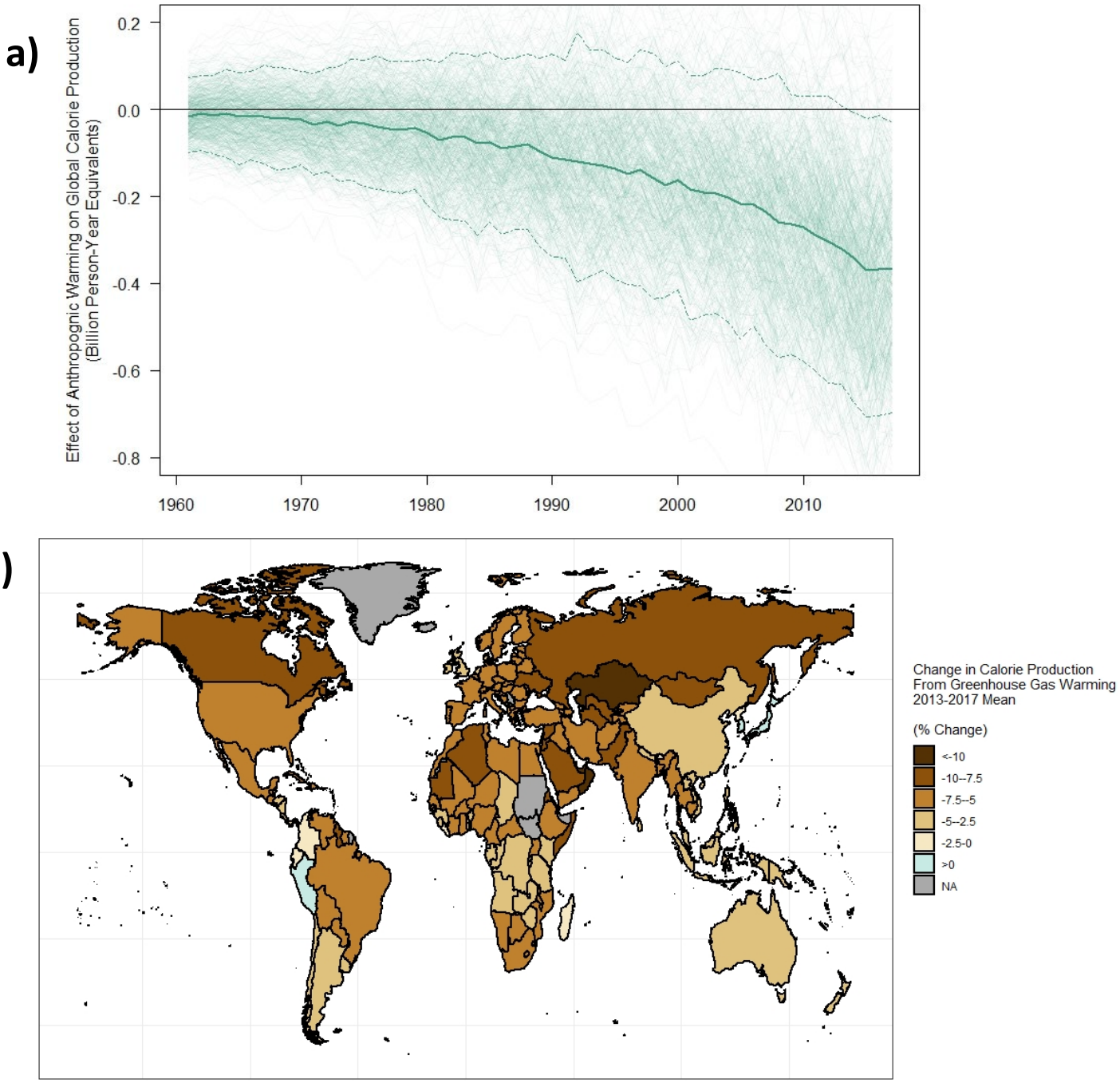

Supplementary Figure 7: Effect of anthropogenic warming on global calorie production. a) Effect of anthropogenic warming on global calorie production from wheat, rice, and maize 1961-2017. Thin lines show 500 draws that randomly sample from the distribution of internal climate variability (via draws from the historical and counterfactual LENS ensembles) and uncertainty in the temperature response to yield (via draws from the parameter distribution of the empirical yield model). Solid line shows the mean effect and dashed lines show the empirical 90% confidence interval. Units are in billion person-year equivalents, assuming a caloric requirement of 2,500 calories per day and allowing for 35% post-harvest losses. b) Distribution of caloric change effect by country (2013-2017 mean, % change relative to observed yields).

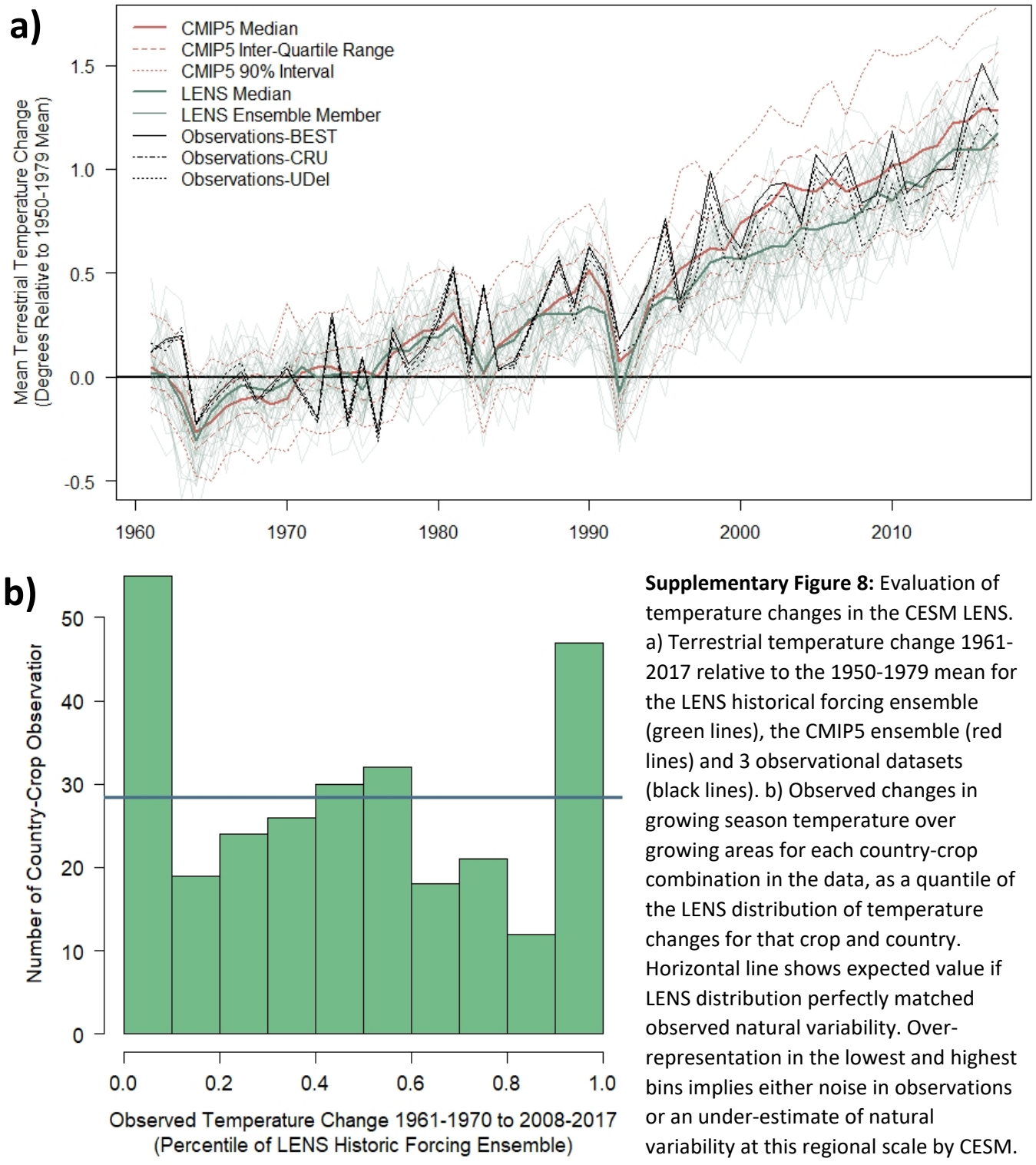

Supplementary Figure 8: Evaluation of temperature changes in the CESM LENS. a) Terrestrial temperature change 1961-2017 relative to the 1950-1979 mean for the LENS historical forcing ensemble (green lines), the CMIP5 ensemble (red lines) and 3 observational datasets (black lines). b) Observed changes in growing season temperature over growing areas for each country-crop combination in the data, as a quantile of the LENS distribution of temperature changes for that crop and country. Horizontal line shows expected value if LENS distribution perfectly matched observed natural variability. Over-representation in the lowest and highest bins implies either noise in observations or an under-estimate of natural variability at this regional scale by CESM.

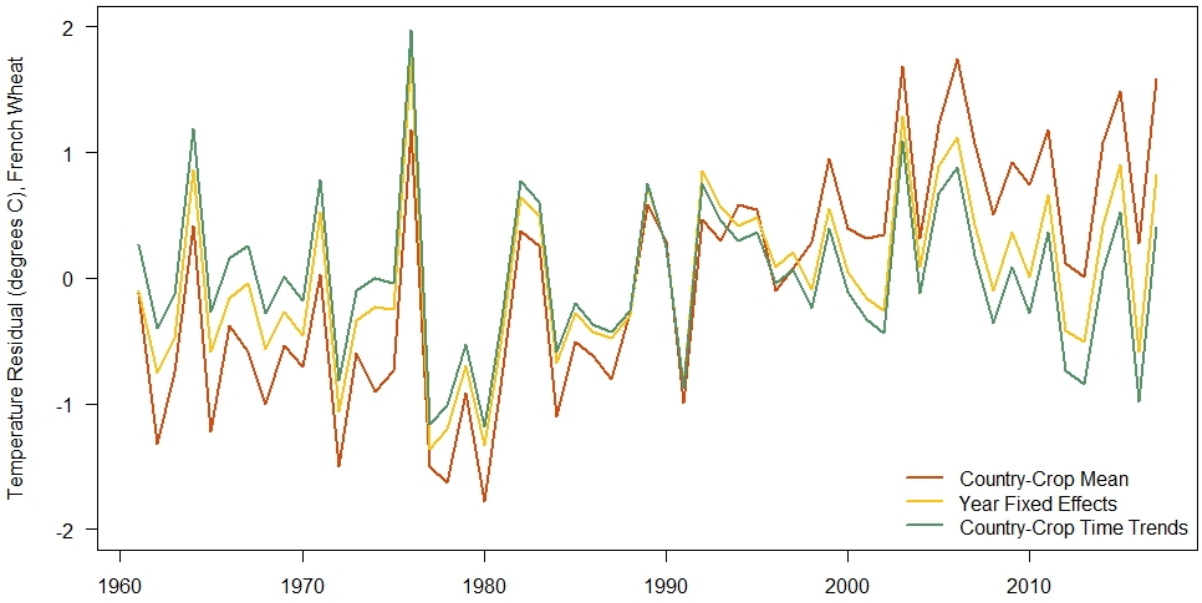

Supplementary Figure 9: Figure showing the effect of regression terms on the variation used to estimate the parameters of the yield-temperature response function (Figure 1 b-d), illustrated using the example of French wheat (i.e. temperatures over wheat growing areas in France, during the French wheat growing season). The raw data (red) shows a strong warming trend of 0.03°C per year ($p<0.001$). Year fixed-effects remove the average global warming effect (yellow line). Since French wheat growing areas are warming slightly faster than the global average, this reduces the warming trend to 0.01°C per year ($p<0.01$) but does not remove it. The addition of country-crop specific quadratic time trends (green line) fully removes the residual warming trend ($p>0.5$). This means that the year fixed-effects, country time trends, and temperature response parameters are to some extent co-determined, a fact that will be reflected in the covariance between these estimated parameters and accounted for in the uncertainty sampling scheme used for the detection and attribution analysis.